Annals of Nuclear Medicine Vol. 20, No. 2, 123–130, 2006

Usefulness of FDG-microPET for early evaluation of therapeutic effects on VX2 rabbit carcinoma

Kentaro ISHII,* Masako N. HOSONO,* Yasuhiro WADA,**,*** Mitsuyo MAEDA,**** Satoko KONDO,* Yoshie TAKADA,* Takuhito TADA,* Terue OKAMURA,***** Yasuyoshi WATANABE**,*** and Yuichi INOUE*

*Department of Radiology, Osaka City University Graduate School of Medicine
**Department of Physiology, Osaka City University Graduate School of Medicine
***RIKEN
****Department of Anatomy, Osaka City University Graduate School of Medicine
*****Saiseikai Nakatsu Hospital

Purpose: The aim of this study was to determine the potential use of high-resolution FDG-microPET for predicting the primary effects of radiotherapy and/or hyperthermia on tumor-bearing rabbits. ***Methods:*** Twenty-eight VX2 xenografts in the thighs of rabbits were divided into the following 5 treatment groups: radiotherapy at a single dose of 10, 20 or 30 Gy, hyperthermia (43 degrees Celsius, 1 hour), and the combination of radiotherapy and hyperthermia (10 Gy + 43 degrees Celsius, 1 hour). FDG-microPET images were obtained by using a microPET P4 system at pretreatment and at 24 hours and 7 days after treatment. For the evaluation by FDG-microPET, tumor/muscle (T/M) ratios, retention index [RI = (T/M ratio at 120 min – T/M ratio at 60 min) / T/M ratio at 60 min], and time activity curve (TAC) were acquired. ***Results:*** We divided the xenografts into a responder group (partial response + stable disease, n = 14) and a non-responder group (progressive disease, n = 14). The T/M ratio at 24 hours after the treatment in the responder group was decreased remarkably with that at pre-treatment ($p < 0.05$), while in the non-responder group it showed no significant change between the time points. The RI and TAC patterns were comparable to T/M ratios in each treatment group. T/M ratios, RI, and TAC indicated marked changes at the time point of 24 hours in the responder group, although the tumors did not show any significant change in volume at that time. Photomicrographs of sections showed that the number of viable tumor cells in the responder group decreased at 24 hours after treatment and that inflammatory cell infiltration was marked and almost all viable tumor cells had disappeared by day 7 after treatment. ***Conclusion:*** These results suggest that early evaluation by FDG-microPET, especially 24 hours after treatment, is useful to predict the primary effects of the treatment. Histological analysis showed that inflammatory cell infiltration at 7 days after treatment was considered to be a cause of accumulation of FDG in the tumors that showed a significant decrease in tumor cell number. This false-positive should be noted when predicting tumor response by FDG accumulation.

Key words: FDG, microPET, radiotherapy, hyperthermia

INTRODUCTION

POSITRON EMISSION TOMOGRAPHY (PET) using ^{18}F-fluoro-deoxyglucose (^{18}F-FDG) has been widely used to differentiate malignant tumors from benign diseases in clinical practice.[1–6] In addition, several studies have suggested the usefulness of FDG-PET for evaluating the effects of various therapies.[7–14] FDG-PET provides metabolic/functional information non-invasively. Accordingly, FDG-PET has been expected to be a predictive tool for evaluating treatment effects. Several clinical studies demonstrated that the early assessment of FDG-PET was informative for predicting the primary effects in the treatment of

Received September 22, 2005, revision accepted November 24, 2005.

For reprint contact: Kentaro Ishii, M,D., Department of Radiology, Osaka City University Graduate School of Medicine, 1–4–3, Asahi-machi, Abeno-ku, Osaka 545–8585, JAPAN.
E-mail: afbxw706@oct.zaq.ne.jp

malignant tumors.[7,8] But they did not show the precise correlation between FDG accumulation and morphologic changes. Furthermore, false-positive or -negative accumulation could occur in the process of necrotic change.[15,16] Therefore, it is necessary to construct an animal model and determine FDG accumulation in association with therapy and examine how it changes as a function of time.

In the present study, we constructed an animal model in which FDG positive tumors were inoculated into rabbits, and used it to assess the FDG uptake in the xenografts after treatment to determine the potential use of high-resolution FDG-microPET in this model for predicting the primary effects of radiotherapy and/or hyperthermia on tumor cells.

MATERIALS AND METHODS

Animal preparation and tumor implantation

All experiments were conducted with prior approval of the Laboratory Animal Center of the Osaka City University Graduate School of Medicine. Japanese white rabbits (weighing 1.8–2.2 kg) were used in this study. VX2 carcinoma cells were supplied from Kyowa Hakko Industry (Tsukuba, Japan) and were maintained as a tumor line in rabbits in our laboratory. Previous study showed transplanted VX2 tumor in the rabbit is an experimental tumor model which is clearly visualized by FDG-PET because the high FDG accumulates to levels several-fold those in normal organs and is thus a suitable model to evaluate the therapeutic effects of anticancer treatment using FDG-PET.[17–20] VX2 carcinomas were inoculated in the bilateral thighs by injection of 0.5 m*l* of tumor suspension (approximately 2×10^7 tumor cells). Our previous study reported the details of tumor implantation.[17] Thirty-two tumors, each about 2 cm in diameter, were used in the experiments.

Radiotherapy and hyperthermia

Eighteen xenografts received irradiation at a single fraction of 10–30 Gy. Six, 4, and 8 xenografts respectively received 10 Gy, 20 Gy, and 30 Gy of irradiation. The rabbits were placed in the supine position and shielded by a whole-body lead cover except for their thighs. In all cases, the xenografts were irradiated with a photon beam (150 kV, 20 mA, Al + Cu filter) at a dose rate of 1.5 Gy/min. Four tumors received thermotherapy. Local hyperthermia was applied by immersion of the tumor-bearing leg in a water bath at 43 degrees Celsius for 1 hour. Six xenografts received combined therapy, both irradiation at a single fraction of 10 Gy and hyperthermia at 43 degrees Celsius for 1 hour. For combined therapy, radiotherapy was given immediately after hyperthermia. Four tumors were not treated (control group). In this study, tumor cell suspension of VX2 was inoculated in the bilateral thighs. The treatment procedure of each xenograft was performed separately. Since the treatment volume was approximately 2 cm in diameter, it was sufficiently small compared to the whole body. Furthermore, the local irradiation and hyperthermia of the thigh were thought to have less influence on the general condition of the rabbit than that of any other site of the body, since the treated site consisted of only the VX2 tumor in the muscle and the femoral bone. Therefore, the animal preparation in this study was thought to be appropriate.

MicroPET and data acquisition

The microPET P4 system (Concorde Microsystems Inc., Knoxville, TN, USA), which evolved from the original University of California at Los Angeles (UCLA) microPET design and has now become commercially available, was used in this study.[21–23] MicroPET with a 2-mm spatial resolution provides sufficient spatial resolution for delineating structures of interest in small laboratory animals.[17,24]

As reported previously,[17] tumor-bearing rabbits were processed for performing transmission scans, under anesthesia with intramuscularly administered ketamine (80 mg)/body and xylazine (8 mg)/body, after a 4-hr fast, and then transmission scans were obtained for 15 min with an 18 MBq ^{68}Ge point source to obtain attenuation correction data. Sequentially, they were administered intravenously 37 MBq/kg body weight of ^{18}F-FDG. Immediately after the FDG injection, the emission data were acquired for 120 min with an energy window of 350–650 keV and a coincidence timing window of 6 ns. The target regions for ongoing microPET studies were bilateral rabbit thighs with transplanted VX2 tumor. The emission list-mode data were sorted into dynamic or static 3D sinograms. All emission scans were corrected for random coincidences

Table 1 Changes in tumor volume following various treatments

treatment	24 hour after treatment*	7 days after treatment*
control	1.50 ± 0.08	9.42 ± 2.01
10 Gy	1.47 ± 0.22	1.98 ± 0.88
20 Gy	1.45 ± 0.11	0.63 ± 0.08
30 Gy	1.44 ± 0.22	0.65 ± 0.10
HT	1.45 ± 0.11	5.62 ± 1.44
HT + 10 Gy	1.43 ± 0.20	2.21 ± 1.01

*Mean ± s.d. Values are comparison of initial tumor volume

Table 2 Changes in T/M ratio following various treatments

treatment	24 hour after treatment*	7 days after treatment*
10 Gy	0.77 ± 0.21	0.88 ± 0.26
20 Gy	0.53 ± 0.10	0.70 ± 0.09
30 Gy	0.58 ± 0.19	0.84 ± 0.44
HT	0.96 ± 0.17	1.09 ± 0.12
HT + 10 Gy	0.65 ± 0.20	0.80 ± 0.22

*Mean ± s.d. Values are comparison of initial tumor T/M ratio

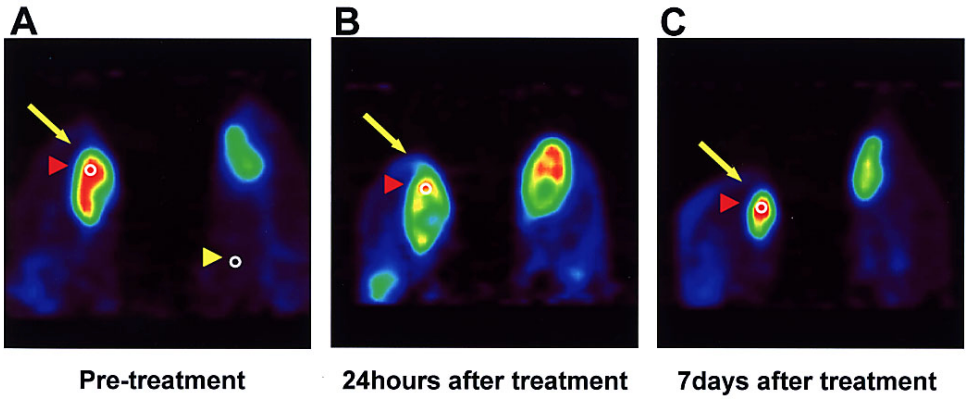

Fig. 1 Coronal FDG-microPET images of the bilateral thighs (tumors were inoculated bilaterally). The VX2 tumor in the responder group after irradiation at a dose of 30 Gy (*arrows*) representing pretreatment (A), 24 hours after treatment (B) and 7 days after treatment (C). Circular ROIs, about 2 mm in diameter, were placed on the area of maximal lesion activity in each of the tumors (*red arrowhead*) and normal muscle. Example of circular ROIs in the normal muscle was shown on panel A (*yellow arrowhead*).

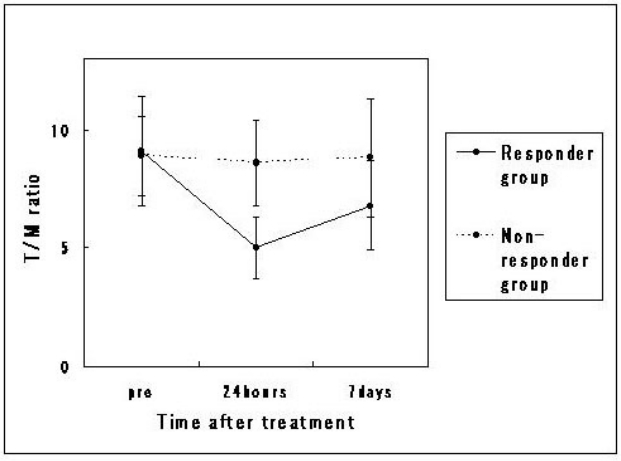

Fig. 2 Relationship between T/M ratio and primary effect. The T/M ratio in the responder group was significantly decreased at 24 hours after treatments ($p < 0.05$).

and normalized for detector efficiencies. The normalized data were collected by the $^{68}Ge/^{68}Ga$ external point source. The attenuation correction data were processed with scatter correction and segmentation due to high scatter fraction in the singles mode. At the segmentation, the threshold value of segmentation was defined manually and segmented into 2 components, i.e., soft tissue and background, whose attenuation coefficients were 0.096 and 0 cm^{-1}, respectively. The attenuation correction data were obtained from the segmented μ-map by forward-projection. Images were reconstructed by a Fourier rebinning (FORE) algorithm and a filtered back-projection (FBP) algorithm with attenuation correction. MicroPET was performed at pretreatment, 24 hours after treatment and 7 days after treatment.

Data analysis

Using PET images, reconstructed by a FBP algorithm using the emission data acquired for 30 min starting 60 min after the FDG injection, tumor FDG uptake between pretreatment, 24 hours after treatment and 7 days after treatment were compared in terms of the tumor/muscle (T/M) ratio. At this time, regions of interest (ROIs) were placed on normal muscles and on areas of tumors showing the maximal lesion activity. The sizes of circular ROIs were 2–4 mm in diameter. The average of 4 ROIs mean values on the muscle of each image was used to obtain the T/M ratios.

For the dynamic study, the emission data were acquired for 120 min after the FDG injection. Based on the emission data, the retention index ([RI = (T/M ratio at 120 min – T/M ratio at 60 min) / T/M ratio at 60 min]) and time activity curve (TAC) were calculated at pretreatment and at 24 hours and 7 days after treatment. The primary effect was determined at 7 days after treatment based on the initial tumor volume. It was previously reported that FDG accumulation in VX2 tumor is well-correlated with the real tumor contour.[25] Also in our former study, VX2 xenograft histologically identified was matched with the FDG accumulation.[17] Therefore, tumor size at pretreatment was calculated by CT and at 7 days after treatment, defined by the histological specimens. Due to institutional regulations, animals injected with radioactivity are not allowed to be taken out from the controlled area. Therefore, tumor size at 24 hours after treatment was optically estimated by FDG-PET imaging. In any case, since the treatment effect itself was not affected by the tumor size at 24 hours after treatment, these different measurement methods were adopted at each time point. All of our experiments were performed in accordance with the governmental and institutional regulations concerning radioactive materials. Data were analyzed using the Wilcoxon

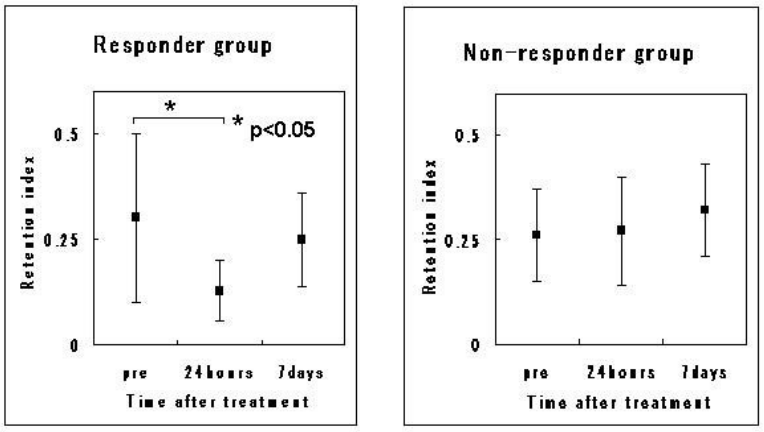

Fig. 3 Relationship between RI (retention index) and primary effect. The RI at 24 hours after treatments in the responder group was significantly lower than that at pre-treatment ($p < 0.05$).

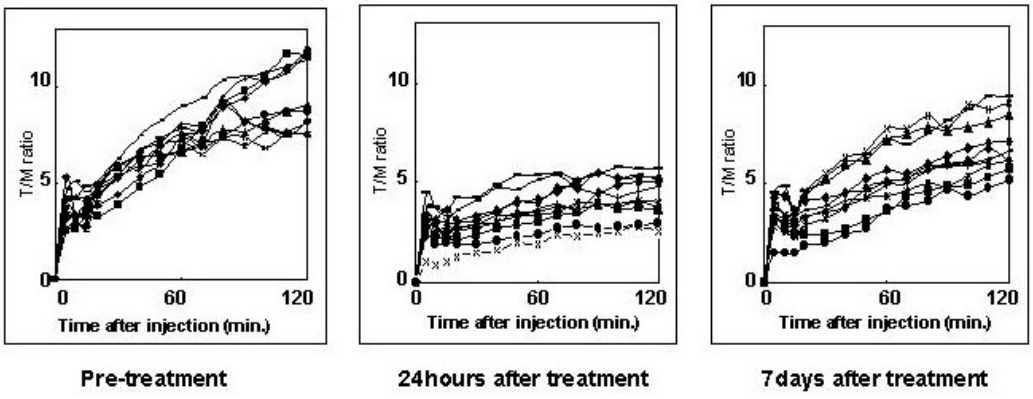

Fig. 4 The TAC of all tumors in the responder group (n = 10). The TAC pattern at 24 hours after the treatment was clearly distinguishable from the TAC pattern at pretreatment and at 7 days after treatment.

signed-rank test, and a probability value of <0.05 was considered significant.

Histological evaluation

PET imaging and results of quantitative analysis were compared with the photomicrographs. For histological evaluation, we prepared 20 treated tumors (4 tumors of each treatment) and the 4 tumors of the control group. Each pathologic specimen was sectioned in the same axial plane as the PET imaging and stained with hematoxylin and eosin. In each treatment group, 2 tumors were sectioned at 24 hours and another 2 at 7 days after treatment.

RESULTS

FDG study

Table 1 shows the tumor volume following the various treatments employed. Although the tumor volume at 7 days after each treatment was different from that of pretreatment and from each other, the tumor volume at 24 hours after treatment had a markedly smaller difference between each treatment group, than at day 7.

Table 2 shows the response, in terms of T/M ratio, to the various treatments employed. Although the T/M ratio of the various treatment groups changed with the treatment intensity, there was no statistically significant difference between any 2 treatment groups. In order to clarify the relationship between early treatment effect and FDG uptake, we divided the xenografts into a responder group (partial response (PR): at least a 50% decrease in the tumor volume + stable disease (SD): less than a 50% decrease or no change in the tumor volume, n = 14) and a non-responder group (progressive disease (PD): an increase in the tumor volume, n = 14). Because of the rapid tumor growth, SD was considered to be in the responder group.

As shown in Figure 1, microPET images clearly demonstrated tumor shapes in the thigh of the rabbit at each time point. In the responder group, the T/M ratio was 5.0 ± 1.3 and 6.8 ± 1.9 at 24 hours and 7 days, respectively, after treatments. In the non-responder group, this ratio was 8.0 ± 3.0, and 8.8 ± 2.5 at each corresponding point. Compared with the T/M ratio at pretreatment (9.1 ± 2.3 in the responder group and 8.9 ± 1.7 in the non-responder group), the ratio in the responder group was remarkably decreased at 24 hours ($p < 0.05$, Fig. 2).

Emission data taken for 120 min after the FDG injection were obtained from 22 xenografts (10 PR + SD and

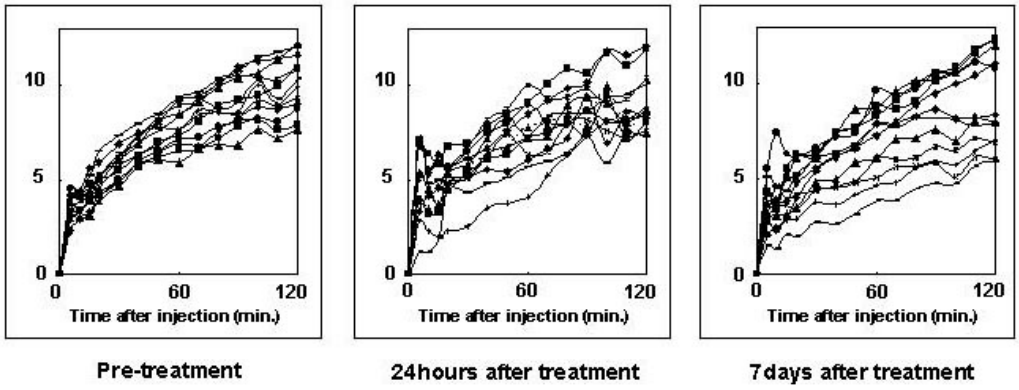

Fig. 5 The TAC of all tumors in the non-responder group (n = 12). There was no difference in the TAC pattern at any time.

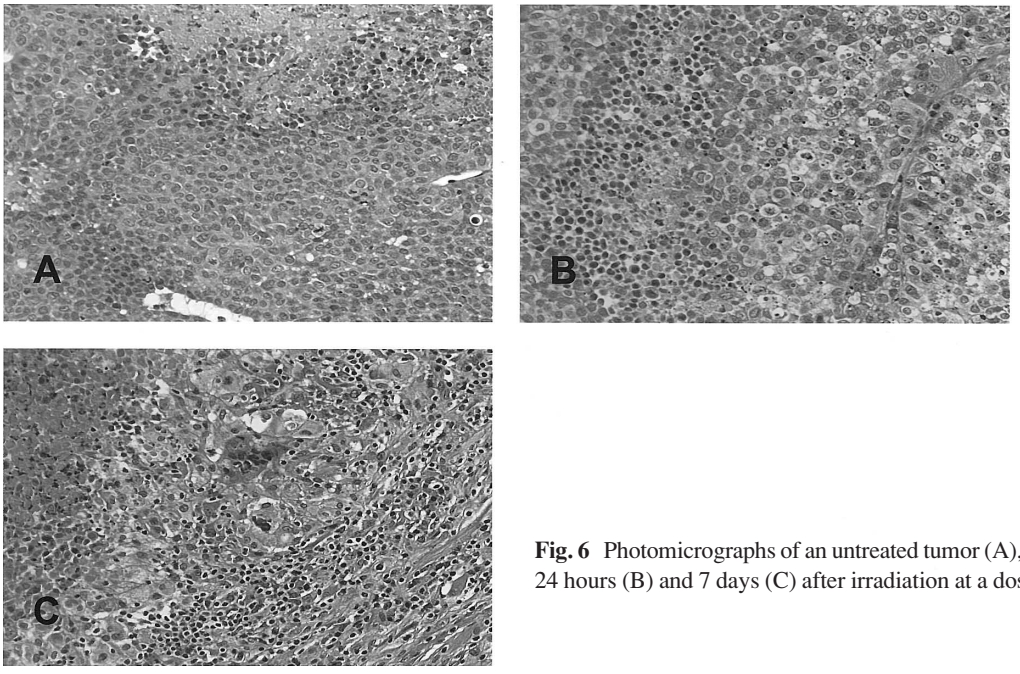

Fig. 6 Photomicrographs of an untreated tumor (A), and tumors 24 hours (B) and 7 days (C) after irradiation at a dose of 30 Gy.

12 PD) to calculate the retention index (RI) and to generate the time activity curve (TAC). In the responder group, the RI was 0.29 ± 0.20, 0.13 ± 0.07, and 0.25 ± 0.11 at pretreatment, 24 hours post treatment, and 7 days post treatment, respectively. The RI at 24 hours after treatments in the responder group was significantly lower than that at pretreatment ($p < 0.05$). In the non-responder group, the RI value was 0.26 ± 0.11, 0.27 ± 0.13, and 0.32 ± 0.11 at pre-treatment, 24 hours post treatment, and 7 days post treatment, respectively. There was no significant difference in the RI between any 2 time points in the non-responder group (Fig. 3).

Figure 4 shows the TAC in the responder group at each time point. In this group, TAC at 24 hours after the treatment remained almost constant over time. It was clearly distinguishable from the TAC pattern at pretreatment and at 7 days after treatment, which kept increasing over time. Figure 5 shows the TAC in the non-responder group at each time point. There was no difference in the TAC pattern at any time. Namely, the early evaluation of the TAC pattern was well correlated with the primary effects. The pattern of TAC was also comparable to the quantitative evaluations of T/M ratios and RI.

Histological study

Photomicrographs of an untreated tumor, and a tumor 24 hours and 7 days after irradiation at a dose of 30 Gy (all tumors with 30 Gy of irradiation were in the responder group) are shown in Figure 6. The untreated tumor consisted of viable VX2 cells and small area of central necrosis. Viable VX2 cells had bright and large nuclei and formed tumor nests (panel A). At 24 hours after treatment, the number of viable tumor cells was markedly decreased, and the residual viable tumor cells showed nuclear

condensation and nuclear collapse, as well as swelling and vacuolization of the cytoplasm. Inflammatory cell infiltration was rarely seen (panel B). In contrast, by 7 days after the treatment, marked central necrosis was seen and the necrotic area was surrounded by marked inflammatory cell infiltration and an increase in the amount of fibrous tissue in addition to the absence of almost all viable tumor cells. Infiltrative inflammatory cells consisted of granulocytes, mononuclear cells (macrophages, lymphocytes and plasma cells), and multinuclear giant cells, which were mainly found around newly formed sites of calcification (panel C). In the non-responder group, there were swelling and vacuolization of the cytoplasm, but neither a decrease in viable tumor cell viability nor inflammatory cell infiltration was seen at any time point. These results are comparable to those from other studies regarding morphologic changes in VX2 carcinomas after radiation therapy and hyperthermia.[24,26–28]

DISCUSSION

Conventional imaging modalities such as computed tomography (CT) or MRI may be inaccurate as an early assessment tool, since morphologic changes may not appear immediately after completion of treatment. Also, tumors containing non-active tissues, such as in the case of fibrosis, necrosis or injured cells, produce a diagnostic dilemma in that the residual mass after treatment does not always equate with the residual disease. On the other hand, FDG-PET has the advantage of detecting changes in glucose metabolism, which are closely related to the viability of the cancer cells. Therefore FDG-PET imaging just after treatment may be useful for early prediction of the treatment outcome.[7,8] The clinical utility of FDG-PET for evaluating the primary effect immediately after the completion of treatment is still controversial, since FDG accumulation in reactive inflammatory cells after treatment may cause a decreased positive predictive value.[15,16]

In the present study, at 24 hours after treatment, although the tumors showed no significant response in terms of volume, the T/M ratios, RI, and TAC were remarkably reduced in the responder group. These results suggest that the evaluation of FDG-PET at 24 hours after treatment is useful to predict primary effects of the treatment in this model. In contrast, despite the fact that the tumor volumes at 7 days after treatment correlated with the applied treatments, tumor FDG uptake showed no significant difference between the responder group and non-responder group at that time. Histological analysis showed that in the responder group the decrease in tumor FDG uptake at 24 hours after treatment was highly related to the decrease in the number of viable tumor cells. Histologically-observed inflammatory cell infiltration at 7 days could explain the accumulation of FDG in tumor tissues that showed a significant decrease in viable tumor cells. A previous study showed the presence of newly formed granulation tissue around the tumor; and macrophages, massively infiltrating the marginal areas surrounding the necrotic area, showed a higher uptake of ^{18}F-FDG than the viable tumor cells.[29] Other authors reported granulocytes and mononuclear cells to have increased glucose utilization at the site of infection.[30,31] Therefore, we suppose that inflammatory cell infiltration could accumulate FDG as much as untreated tumor cells at 7 days after treatment. At 24 hours after treatment, inflammatory cell infiltration had not appeared in the tumor. We conducted this experimental model up to 7 days after treatment, but longer follow-up might detect a decrease in inflammatory cell infiltration, so that in the longer term the tumor FDG uptake might correspond to the response to the treatment. In the non-responder group, many viable tumor cells remained at 24 hours and 7 days after treatments, and FDG uptake at each time point was similar to that for the untreated tumor.

In the responder group, like the T/M ratio, RI and TAC pattern at 24 hours after treatment were clearly distinguishable from those of pre-treatment, and we thus assume that these results reflected a reduced number of viable tumor cells. In contrast, in the responder group at 7 days after treatment, RI and TAC pattern were similar to those at pre-treatment. In light of the histological findings we suppose that active inflammation may contribute to this phenomenon. Whether delayed imaging in FDG-PET enables us to distinguish malignant from inflammatory lesions or not is controversial, since some authors reported that FDG uptake in inflammatory lesion remains stable over time, but other authors reported increases with time.[30,32–36] Although more studies are necessary to further our understanding of these results, our findings suggest that delayed higher tumor uptake may reflect not only tumor cell viability and proliferation but also the contribution of secondary inflammatory reaction elements.

MicroPET could visualize a small radioactive area in the tumor and enabled us to establish this animal model adapted to a clinical setting in the point of ROI calculation. Furthermore, correlations between microPET images and histological specimens were close. MicroPET also has an advantage in evaluating delayed tumor imaging in a small animal model. Since delayed imaging may suffer from higher noise due to the radioactivity decay of ^{18}F, high sensitivity of the PET scanner detector is therefore extremely important; and high sensitivity with 3D data acquisition may be helpful for delayed tumor imaging.

For the quasi-quantitative evaluation of FDG-PET, we used T/M ratios instead of the standardized uptake value (SUV). Our previous investigation of whole-body FDG-PET imaging of rabbits showed more than 50% of prescribed FDG accumulated in the intestine (data not shown). Tatsumi et al.[25] also reported that whole-body FDG-PET imaging of rabbits showed intense FDG accumulation in a portion of the intestines, in addition to the normal brain,

kidneys, bladder, and heart, which exhibited prominent F-18 activity in human FDG-PET imaging. The substantial administered FDG is considered almost half of the actual administered FDG, because of the intense FDG accumulation in the intestine. In addition, FDG uptake of a rabbit intestine is not constant. Consequently, SUV may vary in accordance with the degree of normal FDG distribution such as in intestine. In contrast, FDG accumulation of the muscle was effected by normal FDG distribution in the same manner as tumor site. Therefore, we think that T/M ratio is a relatively stable assessment tool for evaluating tumor FDG uptake in rabbit. However, it is necessary to investigate whether SUV evaluation is appropriate or not in a rabbit tumor model. According to our previous report, plasma glucose level in rabbit was relatively stable, ranging from 96 to 139 mg/d*l* after a 4-hour fast.[17] In this study, although the plasma glucose level was not determined before the FDG injection, FDG-PET scan and data acquisition were performed in the same way as in our previous study.

We established the experimental model described here for examining the usefulness of FDG-PET to predict primary effects after treatment. The evaluation of this experimental model should help establish an early assessment of FDG-PET in clinical practice. Additionally, several differences between the clinical conditions and this experimental model should be noted. First, most clinical tumors are usually irradiated by regimens of fractionated doses, in which cell loss and repopulation occur continuously and inflammatory reaction occurs during treatment. Second, most clinical tumors grow more slowly than those in this experimental model. A tumor cell population with a longer cell cycle will respond later, if mitotic death is the predominant cause of death. Nevertheless, the construction of this experimental model should be an essential step in order to establish an early assessment of FDG-PET in clinical management of malignant tumors.

CONCLUSIONS

In this experimental model, our results suggest that early evaluation of FDG-PET, especially 24 hours after treatment, is useful to predict primary effects of the treatment. Histological analysis showed that the decrease in tumor FDG uptake at 24 hours after treatment was highly related to the decrease in the number of viable tumor cells. Inflammatory cell infiltration at 7 days after treatment was considered to be a cause of FDG accumulation in tumors that showed a significant decrease in viable tumor cells. This false-positive should be noted when predicting tumor responses in terms of FDG accumulation. These investigations should be helpful for the early assessment of FDG-PET in the clinical management of malignant tumors and microPET has a great advantage in evaluating treatment effects in small animals.

ACKNOWLEDGMENTS

The authors thank Dr. Taishi Ohara, Dr. Kouichi Koyama, Dr. Tomohisa Okuma, Dr. Yoshimasa Hamazawa of Osaka City University Graduate School of Medicine for technical assistance and data collection with the FDG-microPET study. They also thank Dr. Larry D. Frye for valuable editorial help.

REFERENCES

1. Kubota K, Matsuzawa T, Fujiwara T, Ito M, Hatazawa J, Ishiwata K, et al. Differential diagnosis of lung tumor with positron emission tomography: a prospective study. *J Nucl Med* 1990; 31: 1927–1932.
2. Di Chiro G. Positron emission tomography using [^{18}F] fluorodeoxyglucose in brain tumors: a powerful diagnostic and prognostic tool. *Invest Radiol* 1987; 22: 360–371.
3. Slosman DO, Spiliopoulos A, Couson F, Nicod L, Louis O, Lemoine R, et al. Satellite PET and lung cancer: a prospective study in surgical patients. *Nucl Med Commun* 1993; 14: 955–961.
4. Gupta NC, Maloof J, Gunel E. Probability of malignancy in solitary pulmonary nodules using fluorine-18-FDG and PET. *J Nucl Med* 1996; 37: 943–948.
5. Demura Y, Tsuchida T, Ishizaki T, Mizuno S, Totani Y, Ameshima S, et al. ^{18}F-FDG accumulation with PET for differentiation between benign and malignant lesions in the thorax. *J Nucl Med* 2003; 44: 540–548.
6. Strauss LG. Fluorine-18 deoxyglucose and false-positive results: a major problem in the diagnostics of oncological patients. *Eur J Nucl Med* 1996; 23: 1409–1415.
7. Torizuka T, Nakamura F, Kanno T, Futatsubashi M, Yoshikawa E, Okada H, et al. Early therapy monitoring with FDG-PET in aggressive non-Hodgkin's lymphoma and Hodgkin's lymphoma. *Eur J Nucl Med Mol Imaging* 2004; 31: 22–28.
8. Koike I, Ohmura M, Hata M, Takahashi N, Oka T, Ogino I, et al. FDG-PET scanning after radiation can predict tumor regrowth three months later. *Int J Radiat Oncol Biol Phys* 2003; 57: 1231–1238.
9. Ichiya Y, Kuwabara Y, Otsuka M, Tahara T, Yoshikai T, Fukumura T, et al. Assessment of response to cancer therapy using fluorine-18-fluorodeoxyglucose and positron emission tomography. *J Nucl Med* 1991; 32: 1655–1660.
10. Guay C, Lepine M, Verreault J, Benard F. Prognostic value of PET using ^{18}F-FDG in Hodgkin's disease for posttreatment evaluation. *J Nucl Med* 2003; 44: 1225–1231.
11. Kostakoglu L, Goldsmith SJ. PET in assessment of therapy response in patients with carcinoma of the head and neck and of the esophagus. *J Nucl Med* 2004; 45: 56–68.
12. Yao M, Graham MM, Hoffman HT, Smith RB, Funk GF, Graham SM, et al. The role of post-radiation therapy FDG PET in prediction of necessity for post-radiation therapy neck dissection in locally advanced head-and-neck squamous cell carcinoma. *Int J Radiat Oncol Biol Phys* 2004; 59: 1001–1010.
13. Hicks RJ, Manus MPM, Matthews JP, Hogg A, Binns D, Rischin D, et al. Early FDG-PET imaging after radical radiotherapy for non-small-cell lung cancer: inflammatory changes in normal tissues correlate with tumor response and do not confound therapeutic response evaluation. *Int J*

Radiat Oncol Biol Phys 2004; 60: 412–418.
14. Gayed I, Vu T, Iyer R, Johnson M, Macapinlac H, Swanston N, et al. The role of ^{18}F-FDG PET in staging and early prediction of response to therapy of recurrent gastrointestinal stromal tumors. *J Nucl Med* 2004; 45: 17–21.
15. Kubota K. From tumor biology to clinical PET: A review of positron emission tomography (PET) in oncology. *Ann Nucl Med* 2001; 15: 471–486.
16. Rege SD, Chaiken L, Hoh CK, Choi Y, Lufkin R, Anzai Y, et al. Change induced by radiation therapy in FDG uptake in normal and malignant structures of the head and neck: Quantitation with PET. *Radiology* 1993; 189: 807–812.
17. Kondo S, Hosono M, Wada Y, Ishii K, Matsumura A, Takada Y, et al. Use of FDG-microPET for detection of small nodules in a rabbit model of pulmonary metastatic cancer. *Ann Nucl Med* 2004; 18: 51–57.
18. Abe Y, Matsuzawa T, Fukuda H, Endo S, Yamada K, Sato T, et al. Experimental study for tumor detection using ^{18}F-2-fluoro-2-deoxy-D-glucose: imaging of rabbit VX2 tumor with single photon gamma camera. *KAKU IGAKU (Jpn J Nucl Med)* 1985; 22: 389–391.
19. Oya N, Nagata Y, Ishigaki T, Abe M, Tamaki N, Magata Y, et al. Evaluation of experimental liver tumors using fluorine-18-2-fluoro-2-deoxy-D-glucose PET. *J Nucl Med* 1993; 34: 2124–2129.
20. Oya N, Nagata Y, Tamaki N, Takagi T, Murata R, Magata Y, et al. FDG-PET evaluation of therapeutic effect on VX2 liver tumor. *J Nucl Med* 1996: 37; 296–302.
21. Cherry SR, Shao Y, Silverman RW. MicroPET: a high resolution PET scanner for imaging small animals. *IEEE Trans Nucl Sci* 1997; 44: 1161–1166.
22. Chatziioannou AF, Cherry SR, Shao Y, Silverman RW, Meadors K, Farquhar TH, et al. Performance evaluation of MicroPET: a high-resolution lutetium oxyorthosilicate PET scanner for animal imaging. *J Nucl Med* 1999; 40: 1164–1175.
23. Tai YC, Chatziioannou A, Siegel S, Young J, Newport D, Goble RN, et al. Performance evaluation of microPET P4: a PET system dedicated to animal imaging. *Phys Med Biol* 2001; 46: 1845–1862.
24. Weber S, Bauer A. Small animal PET: aspects of performance assessment. *Eur J Nucl Med Mol Imaging* 2004; 31: 1545–1555.
25. Tatsumi M, Nakamoto Y, Traughber B, Marshall LT, Geschwind JF, Wahl RL. Initial experience in small animal tumor imaging with a clinical positron emission tomography/computed tomography scanner using 2-[F-18]Fluoro-2-deoxy-D-glucose. *Cancer Res* 2003; 63: 6252–6257.
26. Kim YH, Choi BI, Cho WH, Lim S, Moon WK, Han JK, et al. Dynamic contrast-enhanced MR imaging of VX2 carcinomas after X-irradiation in rabbits. *Invest Radiol* 2003; 38: 539–549.
27. Patricio MB, Soares J, Vilhena M. Morphologic and morphometric studies on tumor necrosis produced by radiotherapy, and hyperthermia singly and in combination. *J Surg Oncol* 1989; 42: 5–10.
28. Nishiue T, Kojima O. Local treatment of rabbit VX2 rectal carcinoma with combined hyperthermia and intratumoral CDDP injection. *Int J Hyperthermia* 1994; 10: 619–626.
29. Kubota R, Yamada S, Kubota K, Ishiwata K, Tamahashi N, Ido T. Intratumoral distribution of fluorine-18-fluorodeoxyglucose *in vivo*: High accumulation in macrophages and granulation tissues studied by microautoradiography. *J Nucl Med* 1992; 33: 1972–1980.
30. Zhuang H, Pourdehnad M, Lambright ES, Yamamoto AJ, Lanuti M, Li P, et al. Dual time point ^{18}F-FDG PET imaging for differentiating malignant from inflammatory processes. *J Nucl Med* 2001; 42: 1412–1417.
31. Yamada S, Kubota K, Kubota R, Ido T, Tamahashi N. High accumulation of fluorine-18-fluorodeoxyglucose in turpentine-induced inflammatory tissue. *J Nucl Med* 1995; 36: 1301–1306.
32. Kubota K, Itoh M, Ozaki K, Ono S, Tashiro M, Yamaguchi K, et al. Advantage of delayed whole-body FDG-PET imaging for tumour detection. *Eur J Nucl Med* 2001; 28: 696–703.
33. Hustinx R, Smith RJ, Benard F. Dual time point fluorine-18 fluorodeoxyglucose positron emission tomography: a potential method to differentiate malignancy from inflammation and normal tissue in the head and neck. *Eur J Nucl Med* 1999; 26: 1345–1348.
34. Lodge MA, Lucas JD, Marsden PK, Cronin BF, O'Doherty MJ, Smith MA. A PET study of ^{18}F-FDG uptake in soft tissue masses. *Eur J Nucl Med* 1999; 26: 22–30.
35. Nakamoto Y, Saga T, Higashi T, Ishimori T, Kobayashi H, Ishizu K, et al. Optimal scan time for evaluating pancreatic disease with positron emission tomography using F-18-fluorodeoxyglucose. *Ann Nucl Med* 2003; 17: 421–426.
36. Ishimori T, Saga T, Mamede M, Kobayashi H, Higashi T, Nakamoto Y, et al. (18)F-FDG uptake in a model of inflammation: concanavalin A-mediated lymphocyte activation. *J Nucl Med* 2002; 43: 658–663.